ARTICLE OPEN

Check for updates

Single-photon pulse induced giant response in $N > 100$ qubit system

Li-Ping Yang [1] and Zubin Jacob [1]✉

The temporal dynamics of large quantum systems perturbed weakly by a single excitation can give rise to unique phenomena at the quantum phase boundaries. Here, we develop a time-dependent model to study the temporal dynamics of a single photon interacting with a defect within a large system of interacting spin qubits ($N > 100$). Our model predicts a quantum resource, giant susceptibility, when the system of qubits is engineered to simulate a first-order quantum phase transition (QPT). We show that the absorption of a single-photon pulse by an engineered defect in the large qubit system can nucleate a single shot quantum measurement through spin noise read-out. This concept of a single-shot detection event ("click") is different from parameter estimation, which requires repeated measurements. The crucial step of amplifying the weak quantum signal occurs by coupling the defect to a system of interacting qubits biased close to a QPT point. The macroscopic change in long-range order during the QPT generates amplified magnetic noise, which can be read out by a classical device. Our work paves the way for studying the temporal dynamics of large quantum systems interacting with a single-photon pulse.

INTRODUCTION

Recent developments in controlling large quantum systems in cold atoms systems[1], ion traps[2], and superconducting qubit systems[3] have opened the new era of quantum simulation. In particular, the study of continuous quantum phase transitions and many-body localization promises to be one of the major applications for quantum computers[4]. Simultaneously, control over large quantum systems allows sensing and parameter estimation with unprecedented sensitivity. In particular, continuous quantum phase transitions combined with repeated measurements can be exploited as a resource for metrology[5,6]. This opens the question whether a giant response can occur in a large quantum system even when weakly perturbed by a single photon[7–10]. Such a system with a giant response can lead to single-shot read-out without the need for repeated measurements.

We develop a time-dependent computational model to study the response of a large quantum system ($N > 100$ qubits) on excitation by a single-photon pulse. We discover a giant response arising from a single photon interacting with a defect state coupled to a large system of collective qubits ($N > 100$), which can function as a quantum amplifier[11]. We believe this striking giant response will motivate experiments of the time dynamics of large quantum systems excited by a single-photon pulse. While we capture the essential physics through a minimalistic model, it points to single-photon nucleated space-time theory of quantum phase transitions where even excited states along with ground states play an important role. This can lead to an exciting frontier at the interface of condensed matter physics and quantum optics. Our proposal can be implemented in a broad range of qubit systems and can lead to devices such as single-photon detectors in spectral ranges inaccessible by current technologies.

We show that giant susceptibility can be exploited as a powerful quantum resource and we overcome two outstanding challenges for the field. Firstly, previous proposals of metrology exploiting second-order QPTs (see Table 1) only give rise to large fidelity susceptibility, not a directly observable quantity. The quantum susceptibility is always low for previously studied second-order QPTs making it detrimental for practical experimental realization. Existing schemes propose to use repetitive measurements on a weak output signal to perform high precision parameter estimation i.e. quantum metrology—fundamentally different from our claim of single-photon pulse driven giant response. For example, in the transverse Ising model, the magnetic susceptibility χ diverges at an extremely low speed with the spin number N ($\chi \sim log(N)$)[12]. Thus, no giant response can be obtained for intermediate-scale quantum systems. On the contrary, the susceptibility diverges with N at the first-order QPT point in our proposed model. Secondly, the time dynamics of a weak signal (e.g., a single-photon pulse) interacting with any large system near a quantum phase transition has never been explicitly demonstrated. We overcome this challenge by exploiting recent developments in quantum pulse scattering theory[13–16].

Exploiting giant quantum susceptibility is an approach fundamentally different from quantum interferometers used for parameter estimation or quantum sensing/metrology[17–19]. The enhanced sensitivity in quantum interferometers benefits from the accumulated phase from a large number of synchronized non-interacting particles in repeated measurements[20–22]. In contrast, the giant sensitivity in our scheme originates from the singular behavior of strongly correlated systems at the phase transition point[11,23]. This giant response can give rise to classical single-shot measurements. In Table 1, we contrast the giant quantum susceptibility proposed in this paper with previously well-known quantum entanglement/squeezing[19,24,25] and quantum criticality[5,6].

The dynamic process of the proposed interacting-qubit system is conceptually similar to the counting events in single-photon avalanche diodes (SPADs) and SNSPDs. This is clarified on contrasting our approach with the well-established and important field of quantum linear amplifiers[26,27]. The gain of linear quantum

[1]Birck Nanotechnology Center and Purdue Quantum Science and Engineering Institute, School of Electrical and Computer Engineering, Purdue University, West Lafayette, IN 47906, USA. ✉email: zjacob@purdue.edu

L.-P. Yang and Z. Jacob

Table 1. Contrast of three fundamental classes of quantum resources.

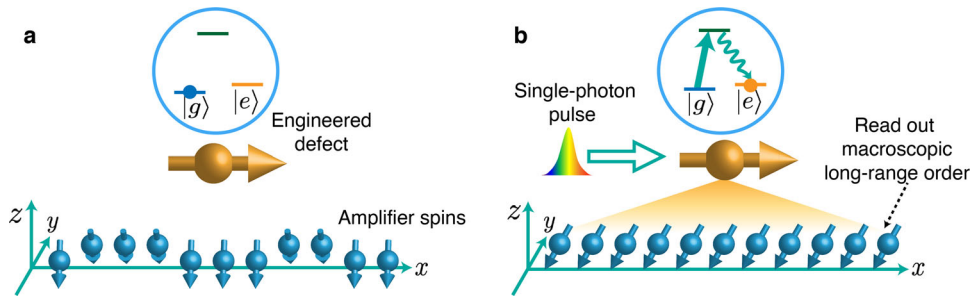| Conceptual basis	Quantum entanglement/squeezing	Quantum criticality	Giant quantum susceptibility
Quantum resource	Based on GHZ[25] or squeezed spin states[24]	Based on second-order (continuous) quantum phase transition[5,6]	Based on first-order (discontinuous) quantum phase transition
Physical mechanism	Heisenberg uncertainty principle	Orthogonality of the ground states of two neighboring quantum phases	Discontinuous change in the long-range spin order
Sensitivity scaling	High phase sensitivity $\partial P/\partial \phi \propto N$ (slope of the population P with respect to the phase ϕ)[19]	High fidelity susceptibility $\partial \mathcal{L}/\partial \lambda \propto N$ (slope of the Loschmidt echo $\mathcal{L} = |\langle G(\lambda)|G(\lambda + \delta\lambda)\rangle|)$[5]	Giant quantum susceptibility $\partial|M|/\partial \lambda \propto N$ (slope of the spontaneous magnetization $|M|$)
Number of measurements	Phase interference based and repetitive measurements required[19]	Repetitive measurements of the decoherence of an ancillary qubit[5]	Single-shot measurement; Non-adiabatic transitions dominate dynamics

Fig. 1 Computational model of single-photon pulse interacting with $N > 100$ qubit system. The interacting spin qubits at the bottom, which can function as a quantum amplifier, are critically biased close to the first-order quantum phase transition (QPT) point. The three states in the absorber on the top form a Λ-structure. After absorption of a single-photon pulse, the absorber is excited from the ground state $|g\rangle$ and finally relaxes to the meta-stable state $|e\rangle$. After the $|g\rangle \rightarrow |e\rangle$ transition, the absorber exerts an effective magnetic field on the amplifier qubits. This magnetic field triggers a QPT in the qubits underneath. Initially, the spin qubits are polarized in the yz-plane (**a**). After the phase transition, the spins rotate to the xz-plane (**b**).

amplifiers arises from the coherent pumping in the ancillary modes. Simultaneously, phase information is encoded in the quadratures of the signal modes which is preserved during the amplification. However, the quantum gain of our system results from the macroscopic change in the order parameter during the QPT. The phase information in the input signal (e.g., the pulse shape) is lost during the amplification and only the pulse number information (0 or 1) is read out by the amplifier.

RESULTS

Working mechanism

We now discuss the working mechanism and implementation of our model. The first step is the transduction (absorption) of the incident single photon in an engineered defect. This process is similar to the generation of the first electron-hole pair in single-photon avalanche diode or the first photo-emission event in the photo-multiplier tube. The highly efficient transduction is realized via a Λ-structure transition as shown in Fig. 1. In contrast to a two-level absorber, this Λ-transition defect has three main benefits: (1) higher absorption probability[28,29]; (2) longer lifetime of the destination state $|e\rangle$[13] conducive for effecient read-out; (3) connection of the optical transition in the absorber and the RF-frequency dynamics in the interacting-qubit system (the amplifier). One promising example of such kind of absorber is a nitrogen-vacancy (NV) center. The states $|g\rangle$ and $|e\rangle$ correspond to the two ground spin states $|0\rangle$ and $|+1\rangle$ of the NV. The T_1 time (lifetime of the state $|e\rangle = |+1\rangle$) of NV centers is few milliseconds at room temperature and even much longer at lower temperatures[30]. The Λ transition can be realized with the spin non-conserving transition[31] as shown in Supplementary Fig. 1 and Supplementary Note 2. After the transduction, the information of the single-photon pulse is written in the $|e\rangle$ state of the absorber.

Amplification is essential to trigger a giant response, since the signal stored in the defect (absorber) after the transduction is usually an extremely weak quantum signal. In our quantum system, the amplifier consists of a large number of interacting ancilla qubits. An important principle is effective engineering of the absorber–amplifier interaction to guarantee that the absorbed energy is transferred to the readout channel to trigger the QPT. In our model, the coupling between the absorber and the amplifier is engineered in x-direction

$$\hat{H}_{int} = B_x |e\rangle\langle e| \sum_{j=1}^{N} \hat{\sigma}_j^x. \tag{1}$$

Due to the large zero-field splitting $\Delta_{gs} \approx 2.87$ GHz between the NV ground spin states $|0\rangle$ and $|\pm 1\rangle$, the coupling to the surrounding spins will not change the NV spin population. Then, the dispersive interaction in Eq. (1) is realized as explained in Supplementary Note 1. This dispersive coupling with strength B_x acts an effective magnetic field for the amplifier qubits[32]. As shown in the following, the defect functions as a control of the QPT in the amplifier. More importantly, the dispersive coupling avoids additional decoherence of the amplifier induced by the single-photon pulse. We note that this Λ-transition transduction framework can also be generalized to a cold-atom or trapped-ion system by employing a specific atom/molecule, which has permanent dipole in the state $|e\rangle$.

In our proposal, the amplification is realized by exploiting the giant sensitivity of the first-order QPT. With the mean-field theory, we predicted a universal first-order QPT in interacting-qubit systems[23]

$$\hat{H}_{Am} = \frac{1}{2}\epsilon \sum_{j=1}^{N} \hat{\sigma}_j^z - \frac{1}{n}\sum_{\langle i<j\rangle}(J_x\hat{\sigma}_i^x\hat{\sigma}_j^x + J_y\hat{\sigma}_i^y\hat{\sigma}_j^y), \tag{2}$$
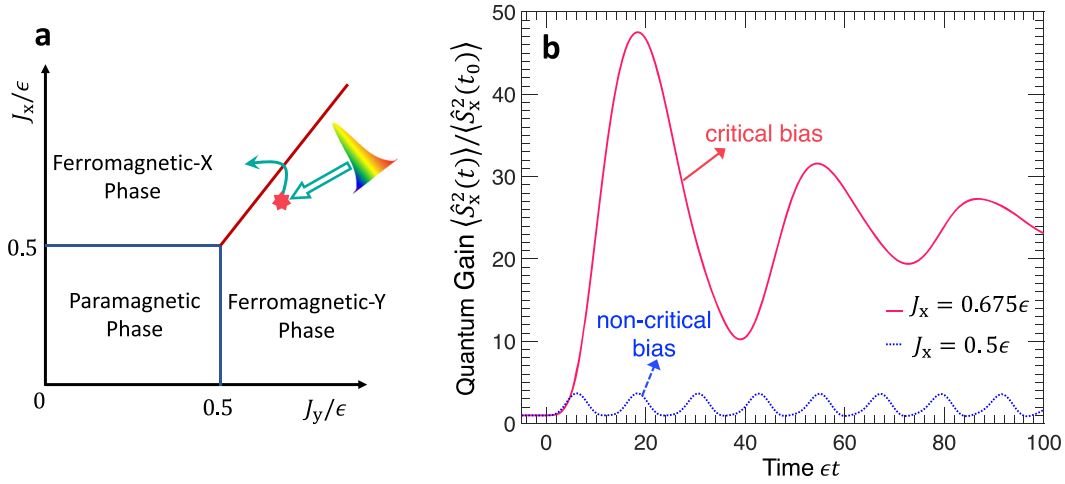
Fig. 2 Single-photon pulse induced first-order quantum phase transition (QPT). a The phase diagram and the initial bias of the amplifier. **b** After absorption of a single-photon pulse, the absorber is flipped to the state $|e\rangle$, on which the absorber exerts a weak magnetic field $B_x \times P_e(t)$ ($P_e(t)$ the population of the state $|e\rangle$) on the amplifier with $N = 400$ qubits. Only if the the amplifier is optically biased around the critical point $J_{x,c} \equiv J_y$, the time varying field can trigger a first-order QPT to obtain a large quantum gain. Here, the qubit-qubit coupling in the y-direction is fixed at $J_y = 0.7$ and the absorber–amplifier coupling $B_x = 0.01\epsilon$.

where ϵ is the energy splitting of the qubits along z direction, J_x and J_y are the strengths of the ferromagnetic qubit-qubit couplings in x- and y-direction respectively, and $\hat{\sigma}_j^a (a = x, y, z)$ are the Pauli matrices of the jth qubit. The summation $\langle i < j \rangle$ runs over n coupled neighbors. For the 1-dimensional Ising chain with $n = 1$, the short-range coupling only exists between the nearest neighbors[33]. For the Lipkin–Meshkov–Glick (LMG) model with $n = N - 1$ (N the total qubit number)[34], all the qubits are coupled with each other.

The amplifier qubits has two ferromagnetic (FM) phases: FM-X and FM-Y with long-range spin order in x- and y-direction. The competition between these two FM phases results in the first-order QPT, which exhibits giant sensitivity for weak signal detection[23]. In Fig. 2a, we present the schematic of the first-order QPT boundary (the red line) in the phase diagram. The quantum phases and the corresponding QPTs can be characterized by two magnetic order parameters

$$\zeta_x \equiv \left\langle \hat{S}_x^2 \right\rangle_0 / N^2 \quad \text{and} \quad \zeta_y \equiv \left\langle \hat{S}_y^2 \right\rangle_0 / N^2, \tag{3}$$

which describe the magnetic fluctuations in the xy-plane. Here, $\hat{S}_a = \sum_j \hat{\sigma}_j^a / 2$ are the collective qubit operators and $\langle \cdots \rangle_0$ means average on the ground-state of the amplifier. The second-order QPTs in interacting-qubit systems have been extensively demonstrated in recent experiments[1–3]. Specifically, the second-order QPT in the LMG model (with long-range qubit-qubit coupling only in x-axis) has also been demonstrated in a recent experiment with 16 dysprosium atoms[35] and strontium atomic ensemble ($N \sim 10^5 - 10^6$) in an optical cavity [36]. We suggest that by adding an additional laser to induce the long-range coupling in y-direction, the first-order QPT due to the competition between the two FM phases can also be observed. This can provide a promising platform to build a single-photon detector utilizing first-order QPT in the LMG model. In the following, we numerically demonstrate the single-photon pulse induced giant response near the first-order QPT of the LMG model, which occurs at $J_x = J_y > \epsilon/2$[23].

The amplification and single-shot readout of the quantum information stored in the state $|e\rangle$ is realized by exploiting the first-order QPT in the amplifier. Initially, the qubit-qubit coupling J_x is pre-biased slightly below the phase transition point $J_{x,c} \equiv J_y$ [see the red star in Fig. 2a] and the amplifier is initialized in its ground state of the FM-Y phase. After absorption of a single-photon pulse, the absorber is flipped to the state $|e\rangle$ with probability $P_e(t)$ (see Supplemental Figs. 1b and 2). Thus, the additional effective

magnetic field experienced by the amplifier qubits is $B_x \times P_e(t)$. The initial critical bias guarantees that the small magnetic field perturbation $B_x \times P_e(t)$ from the absorber can trigger a QPT and leads to efficient amplification.

There are two ways to read out the amplified signal in practice. One is to directly measure the spontaneous magnetization $\sqrt{\zeta_x}$ of the amplifier in x-direction, which increases from an extremely small value to a finite value after the collective rotation of the qubits. Another option is to couple the amplifier qubit with a cavity as proposed in our previous works[11,23]. The energy prestored in the qubits is transferred to the cavity mode generating macroscopic excitations after the QPT. The photons leak out from cavity can be directly measured with classical photodetectors.

Dynamical amplification via quantum phase transition

To characterize the dynamic giant response, we define a time-dependent quantum gain of the amplifier as

$$G(t) = \langle \hat{S}_x^2(t) \rangle / \langle \hat{S}_x^2(t_0) \rangle. \tag{4}$$

We contrast the time-dependent quantum gain for the cases of critical bias (the red-solid curve) and non-critical bias (the blue dotted curve) in Fig. 2b. It is clearly seen that the giant response (corresponding to an efficient amplification) can only be obtained if the system is optimally biased close to the phase transition point[11] (please refer to Supplementary Note 3 and Supplementary Fig. 3a for more details). For fixed weak perturbation $B_x = 0.01\epsilon$, there exist an optimal bias coupling strength $J_x \approx 0.675\epsilon$. We also note that for the critical bias case, the amplifier qubits finally evolve to an excited state in the FM-X phase with macroscopic qubits polarized in xz-plane as shown in following.

To reveal the intrinsic change within the amplifier, we contrast the time-dependent spin Q-function of the amplifier for different biases in Fig. 3. The first row a–d and the second row e–h correspond to critical and non-critical bias cases, respectively. In both cases, the amplifier starts from the FM-Y phase with spin qubits polarized in the yz-plane. The two arms of the Q-function in the yz-plane at time $t_0 = -5/\epsilon$ (the time before the absorption of the pulse) correspond to the two degenerate ground states of the FM-Y phase[23]. For the first row, the incident single-photon pulse triggers a phase transition to the FM-X phase. The qubits rotate 90° to the xz-plane at time $t_0 = 18/\epsilon$ in Fig. 3d. This reveals the dynamic change in the long-range spin order within the amplifier and clearly shows the signature of the detection event. In contrast,
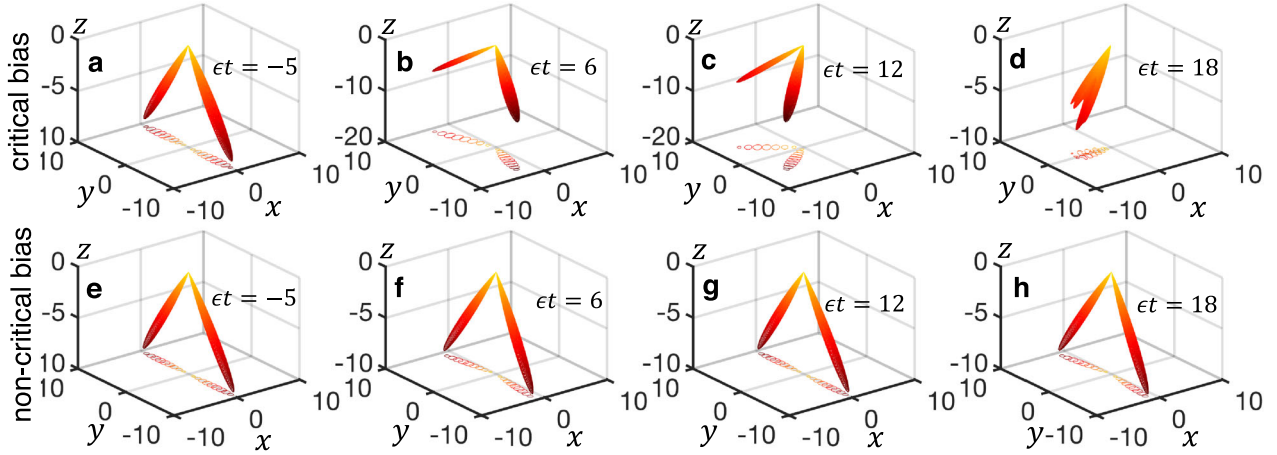
Fig. 3 Dynamics of the amplifier. The spin Q-function characterizes the polarization distribution of the amplifiers qubits. The first rows (**a–d**) shows the dynamic change in the Q-function with bias $J_x = 0.675\epsilon$ very close to the phase transition point $J_{x,c} = J_y = 0.7\epsilon$. The second row (**e–h**) is for the case with $J_x = 0.5\epsilon$ far from $J_{x,c}$. The curves underneath are the contour projections of the corresponding Q-functions in xy-plane.

no macroscopic spin order change occurs when the amplifier is biased far from the phase transition point. The polarization of the spin qubits marginally varies with time in Fig. 3e–h.

Our simulation of the amplifier dynamics has ignored the decoherence of the interacting qubits that may degrade the giant response in practical processes. However, the amplification has completed within the time $\epsilon T_{Am} \approx 15$ (see Supplementary Fig. 3b), which is usually much shorter than the decoherence time of the qubits. If the amplifier is composed of electron spins with typical energy splitting $\epsilon \sim 1$ GHz and coherence time $T_2^* \sim 1$ μs[37], we have $\epsilon T_2^* \approx 1000 \gg \epsilon T_{Am}$. For nuclear spins with typical energy splitting 1 MHz and coherence time $T_2^* \sim 1$ ms at room temperature and longer than 10 s at low temperature[38], the decoherence time is still much longer than the amplification time. With dynamical decoupling techniques[39,40], the coherence time of the spins can be further prolonged 2–3 orders of magnitude[41–43], which is far more than the required time for amplification. The dipole–dipole interaction between the NV center and nuclear spins at the typical distance 1 nm is around 20 kHz. This effective magnetic field ($B_x/\epsilon \approx 0.02$) is large enough to trigger the QPT.

DISCUSSION

The giant response of the interacting qubits fundamentally originates from the singular behaviors of the system at the phase transition point. We now show the singular scalings of the system. We also notice that in most cases, it is difficult for weak input signals to change the coupling strength within the amplifier[11]. Here, we show that a weak magnetic field perturbation can also break the balance of the two FM phase at the phase boundary $J_x = J_y$ to trigger the first-order QPT. This also lays the foundation of the amplification mechanism as shown in the previous section. As shown in the subgraph of Fig. 4a, the order parameter ζ_x (green-dotted line) increases swiftly with the perturbation magnetic field in x-direction and the other order parameter ζ_y (red-solid line) drops. The sensitivity to the magnetic field is characterized by the susceptibility of the spontaneous magnetization

$$\chi = \frac{d\sqrt{\zeta_x}}{dB_x}\bigg|_{B_x \to 0} \propto |B_x|^{-\gamma}, \tag{5}$$

which is symmetric on the two sides of the transition. Here, singular exponent $\gamma \approx 1.525$ is obtained via the numerical calculation. The same susceptibility for the spontaneous magnetization $\sqrt{\zeta_y}$ with respect to a magnetic field in y-axis can also be obtained (data not shown). The susceptibility diverges linearly with the qubit number $\chi \sim N$ as shown in Fig. 4b.
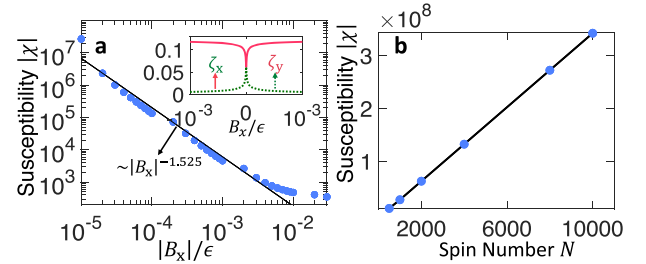

Fig. 4 Singular behavior in the susceptibility. a The susceptibility χ diverges at the phase transition point $J_x = J_y = 0.7\epsilon$. The subgraph shows the abrupt changes in the order parameters in the first-order quantum phase transition with qubit number $N = 1000$. **b** The susceptibility χ near the phase transition point increases linearly with the qubit number N. Here, the perturbation magnetic field is set as $B_x = 10^{-5}\epsilon$.

We emphasize that in first-order QPTs, a singularity occurs on the higher-order magnetic correlation. This is fundamentally different from the traditional thermodynamic phase transitions, in which the diverging spatial correlation length ξ in the microscopic correlator $\langle(\hat{\sigma}_i^x - \langle\hat{\sigma}_i^x\rangle)(\hat{\sigma}_{i+\xi}^x - \langle\hat{\sigma}_{i+\xi}^x\rangle)\rangle$ leads to the divergence of the magnetic susceptibility[44]. However, in the LMG model, the qubits are all coupled with each other with homogeneous strength and the qubits are indistinguishable. Thus, we cannot define a simple correlation length ξ for the LMG model. Alternatively, we define a higher-order correlation function

$$C_{xxyy} = \frac{1}{2}\langle\hat{S}_x^2\hat{S}_y^2 + \hat{S}_y^2\hat{S}_x^2\rangle_0 - \langle\hat{S}_x^2\rangle_0\langle\hat{S}_y^2\rangle_0 \propto |B_x|^{-\tilde{\nu}}, \tag{6}$$

to characterize the macroscopic correlation between the magnetic fluctuations in x- and y-axis.

The diverging C_{xxyy} in the subgraph of Fig. 5a shows the strong negative correlation between $\hat{S}_x^2$ and $\hat{S}_y^2$ at the phase transition point. The negative correlation reveals the fact that the order parameter ζ_y decreases as the other one ζ_x increases. The corresponding singular exponent is $\tilde{\nu} \approx 0.919$ as shown by the black fitting curve. In Supplementary Fig. 4, we show that this exponent is universal for the LMG model, as it is independent on the qubit number N as well as the position on the first-order QPT boundary in Fig. 2. We note that $\tilde{\nu}$ is similar to the traditional correlation length critical exponent[44,45]. We also show that the lower-order correlation $(1/2)\langle\hat{S}_x\hat{S}_y + \hat{S}_y\hat{S}_x\rangle_0 - \langle\hat{S}_x\rangle_0\langle\hat{S}_y\rangle_0$ shows no singularity in Supplementary Note 4.
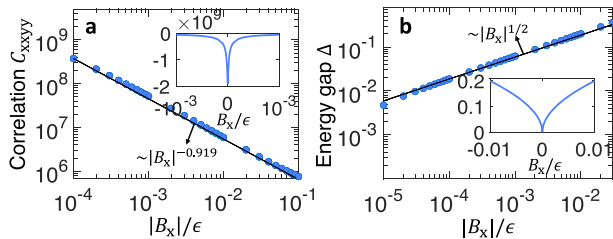
Fig. 5 Singular behavior of the higher-order correlation and energy gap. a The higher-order correlation C_{xxyy} diverges at the phase transition point $J_x = J_y = 0.7\epsilon$. **b** The energy gap vanishes at the phase transition point. The subgraphs show the same curves in the linear coordinates. Both curves are symmetric on the two sides of the phase transition. The solid black lines are the algebraic fittings. The qubit number is set as $N = 1000$.

Another typical character of QPTs is that the energy gap Δ vanishes at the phase transition point as shown in Fig. 5b. The corresponding exponent is given by $\Delta \sim |B_x|^{1/2}$, which is same as the second-order QPT in LMG model[46–48]. The previous study on the size scaling for the LMG model shows that energy gap Δ also vanishes with the increasing qubit number $\Delta \sim 1/N$ at the phase transition point[49,50].

Our work demonstrates the single-photon pulse induced giant response near a first-order QPT point. Our theoretical proposal can be directly implemented in current QPT simulators[1–3]. We note that for microscopic systems, zero temperature generally implies preparing a system in a pure quantum (ground) state. We note, however, that in principle strongly interacting engineered qubits can show QPT behavior at finite temperature environments if the phase transition completes before the decoherence of the system occurs.

Our work paves a way for single-photon detection using quantum phase transition. This defect-controlled-QPT system is based on the fact that the first-order QPT in interaction qubit systems can be induced by a weak in-plane magnetic field. Future work will explore practical implementations on a circuit QED, cold atom and ion trap systems.

DATA AVAILABILITY

The data that support this study are available at https://github.com/yanglp091/QuantumPhaseTransitionDynamics.

CODE AVAILABILITY

The code that supports this study is available at https://github.com/yanglp091/QuantumPhaseTransitionDynamics.

REFERENCES

1. Bernien, H. et al. Probing many-body dynamics on a 51-atom quantum simulator. *Nature* **551**, 579 (2017).
2. Zhang, J. et al. Observation of a many-body dynamical phase transition with a 53-qubit quantum simulator. *Nature* **551**, 601 (2017).
3. Harris, R. et al. Phase transitions in a programmable quantum spin glass simulator. *Science* **361**, 162–165 (2018).
4. Arute, F. et al. Quantum supremacy using a programmable superconducting processor. *Nature* **574**, 505–510 (2019).
5. Quan, H. T., Song, Z., Liu, X. F., Zanardi, P. & Sun, C. P. Decay of loschmidt echo enhanced by quantum criticality. *Phys. Rev. Lett.* **96**, 140604 (2006).
6. Zanardi, P., Paris, M. G. A. & Campos Venuti, L. Quantum criticality as a resource for quantum estimation. *Phys. Rev. A* **78**, 042105 (2008).

7. Lü, X.-Y., Zheng, Li-Li, Zhu, G.-L. & Wu, Y. Single-photon-triggered quantum phase transition. *Phys. Rev. Appl.* **9**, 064006 (2018).
8. Shahmoon, E., Wild, D. S., Lukin, M. D. & Yelin, S. F. Cooperative resonances in light scattering from two-dimensional atomic arrays. *Phys. Rev. Lett.* **118**, 113601 (2017).
9. Wang, Y. et al. Single-photon bound states in atomic ensembles arXiv:1809.01147. Preprint at https://arxiv.org/abs/1809.01147 (2018).
10. Fink, T., Schade, A., Höfling, S., Schneider, C. & Imamoglu, A. Signatures of a dissipative phase transition in photon correlation measurements. *Nat. Phys.* **14**, 365–369 (2018).
11. Yang, L.-P. & Jacob, Z. Quantum critical detector: amplifying weak signals using discontinuous quantum phase transitions. *Opt. Express* **27**, 10482–10494 (2019a).
12. Um, J., Lee, S.-Ik & Kim, B. J. Quantum phase transition and finite-size scaling of the one-dimensional ising model. *J. Korean Phys. Soc.* **50**, 285 (2007).
13. Yang, L.-P., Tang, H. X. & Jacob, Z. Concept of quantum timing jitter and non-markovian limits in single-photon detection. *Phys. Rev. A* **97**, 013833 (2018).
14. Yang, L.-P., Khandekar, C., Li, T. & Jacob, Z. Single photon pulse induced transient entanglement force. *N. J. Phys.* **22**, 023037 (2020).
15. Baragiola, B. Q., Cook, R. L., Brańczyk, A. M. & Combes, J. n-photon wave packets interacting with an arbitrary quantum system. *Phys. Rev. A* **86**, 013811 (2012).
16. Wang, Y., Minář, J., Sheridan, L. & Scarani, V. Efficient excitation of a two-level atom by a single photon in a propagating mode. *Phys. Rev. A* **83**, 063842 (2011).
17. Degen, C. L., Reinhard, F. & Cappellaro, P. Quantum sensing. *Rev. Mod. Phys.* **89**, 035002 (2017).
18. Demkowicz-Dobrzański, R., Kołodyński, J. & Guţă, M. The elusive heisenberg limit in quantum-enhanced metrology. *Nat. Commun.* **3**, 1063 (2012).
19. Giovannetti, V., Lloyd, S. & Maccone, L. Quantum-enhanced measurements: beating the standard quantum limit. *Science* **306**, 1330–1336 (2004).
20. Zhang, J. et al. Noon states of nine quantized vibrations in two radial modes of a trapped ion. *Phys. Rev. Lett.* **121**, 160502 (2018).
21. Davis, E., Bentsen, G. & Schleier-Smith, M. Approaching the heisenberg limit without single-particle detection. *Phys. Rev. Lett.* **116**, 053601 (2016).
22. Thorne, K. S. Nobel lecture: Ligo and gravitational waves iii. *Rev. Mod. Phys.* **90**, 040503 (2018).
23. Yang, L.-P. & Jacob, Z. Engineering first-order quantum phase transitions for weak signal detection. *J. Appl. Phys.* **126**, 174502 (2019b).
24. Wineland, D. J., Bollinger, J. J., Itano, W. M. & Heinzen, D. J. Squeezed atomic states and projection noise in spectroscopy. *Phys. Rev. A* **50**, 67–88 (1994).
25. Bollinger, J. J., Itano, W. M., Wineland, D. J. & Heinzen, D. J. Optimal frequency measurements with maximally correlated states. *Phys. Rev. A* **54**, R4649–R4652 (1996).
26. Caves, C. M., Combes, J., Jiang, Z. & Pandey, S. Quantum limits on phase-preserving linear amplifiers. *Phys. Rev. A* **86**, 063802 (2012).
27. Bergeal, N. et al. Analog information processing at the quantum limit with a josephson ring modulator. *Nat. Phys.* **6**, 296 (2010).
28. Pinotsi, D. & Imamoglu, A. Single photon absorption by a single quantum emitter. *Phys. Rev. Lett.* **100**, 093603 (2008).
29. Young, S. M., Sarovar, M. & Léonard, F. Fundamental limits to single-photon detection determined by quantum coherence and backaction. *Phys. Rev. A* **97**, 033836 (2018).
30. Jarmola, A., Acosta, V. M., Jensen, K., Chemerisov, S. & Budker, D. Temperature- and magnetic-field-dependent longitudinal spin relaxation in nitrogen-vacancy ensembles in diamond. *Phys. Rev. Lett.* **108**, 197601 (2012).
31. Chu, Y., Markham, M., Twitchen, D. J. & Lukin, M. D. All-optical control of a single electron spin in diamond. *Phys. Rev. A* **91**, 021801 (2015).
32. Zhao, N., Hu, J.-L., Ho, S.-W., Wan, J. T. K. & Liu, R. B. Atomic-scale magnetometry of distant nuclear spin clusters via nitrogen-vacancy spin in diamond. *Nat. Nanotechnol.* **6**, 242 (2011).
33. Sachdev, S. *Quantum Phase Transitions* (Wiley Online Library, 2007).
34. Lipkin, H. J., Meshkov, N. & Glick, A. J. Validity of many-body approximation methods for a solvable model:(i). exact solutions and perturbation theory. *Nucl. Phys.* **62**, 188–198 (1965).
35. Makhalov, V. et al. Probing quantum criticality and symmetry breaking at the microscopic level. *Phys. Rev. Lett.* **123**, 120601 (2019).
36. Muniz, J. A. et al. Exploring dynamical phase transitions with cold atoms in an optical cavity. *Nature* **580**, 602–607 (2020).
37. Ryan, C. A., Hodges, J. S. & Cory, D. G. Robust decoupling techniques to extend quantum coherence in diamond. *Phys. Rev. Lett.* **105**, 200402 (2010).
38. Yang, S. et al. High-fidelity transfer and storage of photon states in a single nuclear spin. *Nat. Photonics* **10**, 507 (2016a).
39. Zhao, N., Ho, S.-W. & Liu, R.-B. Decoherence and dynamical decoupling control of nitrogen vacancy center electron spins in nuclear spin baths. *Phys. Rev. B* **85**, 115303 (2012).
40. Yang, W., Ma, W.-L. & Liu, R.-B. Quantum many-body theory for electron spin decoherence in nanoscale nuclear spin baths. *Rep. Prog. Phys.* **80**, 016001 (2016b).

41. Balasubramanian, G. et al. Ultralong spin coherence time in isotopically engineered diamond. *Nat. Mater.* **8**, 383 (2009).
42. Ladd, T. D., Maryenko, D., Yamamoto, Y., Abe, E. & Itoh, K. M. Coherence time of decoupled nuclear spins in silicon. *Phys. Rev. B* **71**, 014401 (2005).
43. Maurer, P. C. et al. Room-temperature quantum bit memory exceeding one second. *Science* **336**, 1283–1286 (2012).
44. Kardar, M. *Statistical Physics of Fields* (Cambridge University Press, 2007).
45. Dziarmaga, J. Dynamics of a quantum phase transition and relaxation to a steady state. *Adv. Phys.* **59**, 1063–1189 (2010).
46. Defenu, N., Enss, T., Kastner, M. & Morigi, G. Dynamical critical scaling of long-range interacting quantum magnets. *Phys. Rev. Lett.* **121**, 240403 (2018).
47. Xue, M., Yin, S. & You, L. Universal driven critical dynamics across a quantum phase transition in ferromagnetic spinor atomic bose-einstein condensates. *Phys. Rev. A* **98**, 013619 (2018).
48. Ribeiro, P., Vidal, J. & Mosseri, R. Exact spectrum of the lipkin-meshkov-glick model in the thermodynamic limit and finite-size corrections. *Phys. Rev. E* **78**, 021106 (2008).
49. Botet, R. & Jullien, R. Large-size critical behavior of infinitely coordinated systems. *Phys. Rev. B* **28**, 3955–3967 (1983).
50. Dusuel, S. & Vidal, J. Continuous unitary transformations and finite-size scaling exponents in the lipkin-meshkov-glick model. *Phys. Rev. B* **71**, 224420 (2005).

ACKNOWLEDGEMENTS

AUTHOR CONTRIBUTIONS

L.P.Y and Z.J. conceived the idea and wrote the manuscript. L.P.Y performed the calculation under the supervision of Z.J.

COMPETING INTERESTS

The authors declare no competing interests.

ADDITIONAL INFORMATION

Supplementary information is available for this paper at https://doi.org/10.1038/s41534-020-00306-w.

Correspondence and requests for materials should be addressed to Z.J.

Reprints and permission information is available at http://www.nature.com/reprints

Publisher's note Springer Nature remains neutral with regard to jurisdictional claims in published maps and institutional affiliations.